Chapter 12
Accurate Hydrodynamic Modeling with the Boundary Element Method

Sergio R. Aragon

Abstract The integral equations of hydrodynamics are presented for both stick and slip boundary conditions, and results of computations including rigid amino acids are used to obtain a new interpretation of the significance of the hydration parameter used in hydrodynamic modeling. The dynamics of the protein surface perturbs water at that boundary, giving rise to additional viscous energy dissipation which is mimicked by a uniform solvation of 1.1 A thick with stick boundary conditions. BEST (Aragon SR, J Comput Chem 25:1191–12055, 2004) has been used to study 49 different proteins, ranging in molecular weight from 9 to 400 kDa, and we have shown that a model using a 1.1 A thick hydration layer describes all protein transport properties very well. Molecular dynamics (MD) simulation has been used to investigate the origin of a handful of significant discrepancies in some multimeric proteins. A preliminary study of dimeric α-chymotrypsin using approximate implicit water MD is presented. In addition I describe the successful validation of modern protein force fields, ff03 and ff99SB, for the accurate computation of solution structure in explicit water simulation for small proteins using trajectories around 10 ns duration. We have also studied a 150 kDa flexible monoclonal IgG antibody, trastuzumab, with multiple independent trajectories encompassing over 320 ns of simulation. The close agreement within experimental error of the computed and measured properties allows us to conclude that MD does produce structures typical of those in solution and that flexible molecules can be properly described using the method of ensemble averaging over a trajectory.

Keywords Boundary elements • Hydrodynamics • Protein molecular dynamics • Diffusion • Intrinsic viscosity

S.R. Aragon (✉)
Department of Chemistry, San Francisco State University, San Francisco, CA, USA
e-mail: aragons@sfsu.edu

S. Uchiyama et al. (eds.), *Analytical Ultracentrifugation*,
DOI 10.1007/978-4-431-55985-6_12

12.1 Introduction

Hydrodynamic modeling plays an important role in the interpretation and study of global molecular motion in liquids. A large number of experimental techniques measure relaxations which include global molecular motions (Aragon 2011). An important method apart from these purely spectroscopic methods is ultracentrifugation. This technique induces the molecule to flow in the presence of a centrifugal field, and its steady-state drift is carefully measured to obtain the sedimentation coefficient (Richards 1980). The sedimentation coefficient is proportional to the average translational diffusion coefficient D and includes a term that contains the specific volume of the molecule in question, but D can be measured directly from the broadening of the sedimentation boundary. Great advances have been made in ultracentrifugation in recent times allowing the deconvolution of mixtures of several molecules (Schuck 2000). As experimental techniques advance in precision, a greater need in accuracy and precision in hydrodynamic modeling arises for the proper interpretation of experimental measurements that depend on hydrodynamic transport properties.

There are three different methodologies to compute hydrodynamic transport properties. The most well-established method is the hydrodynamic interacting bead methodology for the solution of mobility problems. This methodology is discussed at length in Chaps. 10 and 11 of this volume. The second methodology is the boundary element method (BE) – the subject of this chapter (note that Chap. 11 also discusses a graphical interface for BEST within the US-SOMO software). The third methodology, like the BE method, is relatively new – the diffusive Monte Carlo approach (Kang et al. 2004). This last method is not capable of computing tensor values of hydrodynamic transport coefficients, and is most useful for the computation of the average translational diffusion coefficient, but it can handle flexible molecules and provide a decent approximation to the intrinsic viscosity (see also http://web.stevens.edu/zeno/). In this chapter the boundary element method is presented in detail and the differences with the bead methodology are briefly highlighted.

The Stokes creeping flow equations represent the solvent as a mathematical continuum for the case of an incompressible fluid at very low Reynolds number. These differential equations can be solved exactly as a boundary value problem for only a few systems with smooth boundaries: the triaxial ellipsoid (and its degenerate brethren such as a sphere), the toroid, and the dumbbell (Kim and Karilla 1991). To represent a molecule of an arbitrary shape, the early workers (Bloomfield et al. 1967; Garcia de la Torre and Bloomfield 1977a; Teller et al. 1979) used an assembly of beads, at first as a coarse-grained representation. In bead modeling the hydrodynamic interaction of two spheres is given in general as an infinite series expansion in the distance between the spheres. When that distance between spheres exceeds the sum of the diameters, the tensor to first order in the bead size for stick boundary conditions is given by a variational expression first obtained by Rotne and Prager (Rotne and Prager 1969) for the case of equal

diameter spheres, which was later generalized to two unequal bead sizes (Garcia de la Torre and Bloomfield 1977b). However, when atomistic resolution is attempted, a problem arises – there does not exist a hydrodynamic interaction tensor for unequal diameter spheres. This has led bead modelers to use a basic approximation: resize spheres to make them of equal diameter if they overlap (Garcia de la Torre et al 2000a) or, even more coarsely, assign a single atomic effective radius (AER) to all the heavy atoms of a molecule in order to avoid this problem (Garcia de la Torre et al 2000b). Other workers have produced variants of the bead methodology, including clever techniques such as the AtoB program to go from an atomistic representation of a protein to a bead representation with control of the degree of coarseness (Byron 1997). Another prominent bead implementation is the SOMO program (Rai et al 2005; Brookes et al. 2010) which is incorporated in the UltraScan sedimentation analysis package. A slightly different bead methodology has also been proposed (Durchschlag and Zipper 2003). The bead methodology is successful to a certain degree – the results are generally not accurate enough to correctly interpret subtle effects of hydration or molecular conformation that other more accurate hydrodynamic treatments are able to handle. In addition, Goldstein has fully explained why the typical implementations of bead hydrodynamics fail to give correct answers for the rotational diffusion of linear bead assemblies and why such programs thus need the "volume correction" (Goldstein 1985). An early implementation of bead methodology (Spotorno et al. 1997) actually included a module to perform correct Goldstein hydrodynamics, but the routine was not included in the later incarnation of what became the SOMO program. This appears to be the case in most bead implementations used at the present time, including all the work from the Garcia de la Torre group. In the boundary element method, the issues of bead overlaps or volume corrections do not arise because the computation focuses exclusively on the hydrodynamic surface represented as interacting triangles instead of beads. As a result, BE calculations are extremely accurate.

An implementation of the BE method was first provided in hydrodynamics in 1975 (Youngren and Acrivos 1975a), even though the basic mathematics was known much earlier (Odqvist 1930). These authors pointed out that the Stokes equations, ordinarily written as partial differential equations with specified boundary conditions, could also be written down exactly as an integral equation for the velocity field outside an arbitrarily shaped body and implemented an algorithm for its solution. In addition, in integral equation form, it is a simple matter to treat stick, slip, or a mixture of the two boundary conditions because they are incorporated into the integral equation (Youngren and Acrivos 1975a; Hu and Zwanzig 1974; Allison 1999). In bead methodology, a rigorous treatment of the slip boundary condition does not exist and only ad hoc approximations have been attempted so far (Venable and Pastor 1988). In the BE method, the starting equation is exact, as was emphasized much later (Wegener 1986), while in the bead methodology, the hydrodynamic interaction tensors are approximate.

The integral equation of hydrodynamics is a Fredholm integral equation of the first kind. Kim and Karilla expounded at length in their modern micro-hydrodynamics treatise about the pitfalls of using this equation due to the fact that

it is ill-conditioned (Kim and Karilla 1991). These authors developed a complex methodology in order to overcome this difficulty – the completed double layer boundary integral method, which has not found much favor so far. The integral equation is ill-conditioned because the hydrodynamic interaction matrix that arises when the integral equation is discretized has a zero eigenvalue due to the condition that the Oseen tensor has zero divergence. Such an eigenvalue makes the matrix singular and not invertible. This accounts for the observation of early implementers of the BE method (Allison 1999) that as the number of surface elements increased, the results of the BE method decreased in quality. Essentially, the round-off error in the matrix computation allowed it to be invertible for small sizes but as the matrix size increases, instability arises. However, Aragon published a new implementation of the BE method for stick boundary conditions in which a robust regularization method was incorporated in a program called BEST (Aragon 2004). This allowed the solution of the Stokes equations to unprecedented accuracy, as was amply demonstrated in a recent review (Aragon 2011). In that review it is shown that the BE computations can be as accurate and precise as full analytical solutions for the case when such solutions exist.

This chapter is organized as follows. In Sect. 12.2, the integral equation of hydrodynamics is presented and its solution for either stick or slip boundary conditions via the BE method is discussed. In Sect. 12.3, a thorough discussion is given on the significance of the hydration parameter that is used in all hydrodynamic modeling methods with an eye toward identifying the important contributions of the macromolecule in the determination of this parameter. In Sect. 12.4, a review of the accuracy of the BE method is presented with an emphasis on translational diffusion by a variety of experimental methods and the intrinsic viscosity. Outstanding problems with multimeric proteins are described. In Sect. 12.5, a review of the successful treatment of flexible antibodies in conjunction with molecular dynamics simulations is presented. It should be mentioned that even though this volume is mainly concerned with the sedimentation coefficient, we will discuss translation, rotation, and intrinsic viscosity in our effort to demonstrate that a properly formulated hydrodynamic model must yield accurate results using the same parameters for all transport properties, not just translation.

12.2 The Integral Equations of Stokes Flow

For solute molecules larger than the solvent, consideration of the solvent as a continuum is an excellent approximation, and the governing equations, in the limit of small Reynolds number appropriate for the diffusion process, are known as the Stokes or creeping flow equations (Kim and Karilla 1991). Whereas bead methods aim to directly solve a mobility problem which cannot be formulated exactly, an alternative method is to solve a resistance problem which can be formulated exactly as an integral equation. As is shown below, once one has precise friction tensors, it is straightforward to compute the mobility: the diffusion tensors.

12.2.1 Stick Boundary Conditions

For the case of macromolecules in aqueous solution, "stick" boundary conditions are appropriate [but see Sect. 12.3 below for a discussion of why this is so]. In stick boundary conditions, the velocity vector of the fluid at the body surface is zero, i.e., the solvent moves with the body. In this case, the velocity field of the flow, $v(y)$ at position y in the fluid, can be written exactly as an integral over the particle surface (SP):

$$\mathbf{u}(\mathbf{y}) = \mathbf{u}_0(\mathbf{y}) + \oiint \mathbf{T}(\mathbf{x}, \mathbf{y}).\mathbf{f}(\mathbf{x}) dS_x \tag{12.1}$$

where $\mathbf{u}_o(\mathbf{y})$ is the flow velocity of the fluid if the particle was not there (which can be taken to be zero for diffusive motion) and $\overleftrightarrow{\mathbf{T}}(\mathbf{x}, \mathbf{y})$ is the Oseen hydrodynamic interaction tensor. The surface stress force, $\mathbf{f}(\mathbf{x})$, is the unknown quantity that we must obtain. Once this quantity is known, the transport properties of the macromolecule can be directly computed, as shown below. The Oseen tensor (Oseen 1927; Kim and Karilla 1991) given by

$$\mathbf{T}(\mathbf{x}, \mathbf{y}) = \frac{1}{8\pi\eta\,|\mathbf{x}-\mathbf{y}|}\left[\mathbf{I} + \frac{(\mathbf{x}-\mathbf{y})(\mathbf{x}-\mathbf{y})}{|\mathbf{x}-\mathbf{y}|^{\,2}}\right] \tag{12.2}$$

is an exact representation of the hydrodynamic interaction of the infinitesimal surface elements. The solvent viscosity is η. Thus the starting expressions for the calculation, unlike the bead modeling case, are exact; moreover, the equation is applicable to bodies of arbitrary shape.

Since Eq. (12.1) is an integral equation, the solution requires the discretization of the particle surface. The method, however, can be iterated to obtain arbitrary precision. The surface is discretized by replacing it with a collection of N patches that smoothly tile the molecular surface. The details of the solution have been presented previously (Aragon 2004; Aragon 2011). The solution of a linear system of equations containing a superposition of hydrodynamic interactions between the surface patches yields the unknown surface stress force, from which the overall frictional force and torque on the body are computed. Since the velocities and angular velocities are known, the 6×6 friction tensor can be extracted from the total force and torque. The 6×6 friction tensor is composed of 4 3×3 blocks: $\overleftrightarrow{\mathbf{K}}_{tt}$, $\overleftrightarrow{\mathbf{K}}_{tr}$, $\overleftrightarrow{\mathbf{K}}_{rt}$, $\overleftrightarrow{\mathbf{K}}_{rr}$. There are actually only three independent 3×3 friction tensors because the translation-rotation coupling $\overleftrightarrow{\mathbf{K}}_{tr}$ tensor is the transpose of the $\overleftrightarrow{\mathbf{K}}_{rt}$ tensor. This coupling is small unless the body has a screwlike axis of symmetry (Brenner 1967). The 6×6 translation-rotation diffusion tensor is given exactly as the inverse of the 6×6 complete friction tensor whose four 3×3 blocks are the $\overleftrightarrow{\mathbf{K}}$ mentioned above. It is straightforward to show that the 3×3 diagonal blocks of the complete diffusion tensor can be obtained from the friction tensors by an easy 3×3

matrix inversion:

$$\overleftrightarrow{\mathbf{D}}_{\mathrm{tt}} = kT\left[\overleftrightarrow{\mathbf{K}}_{\mathrm{tt}} - \overleftrightarrow{\mathbf{K}}_{\mathrm{tr}}.\overleftrightarrow{\mathbf{K}}_{\mathrm{rr}}^{-1}.\overleftrightarrow{\mathbf{K}}_{\mathrm{rt}}\right]^{-1} \tag{12.3}$$

$$\overleftrightarrow{\mathbf{D}}_{\mathrm{rr}} = kT\left[\overleftrightarrow{\mathbf{K}}_{\mathrm{rr}} - \overleftrightarrow{\mathbf{K}}_{\mathrm{tr}}.\overleftrightarrow{\mathbf{K}}_{\mathrm{tt}}^{-1}.\overleftrightarrow{\mathbf{K}}_{\mathrm{rt}}\right]^{-1} \tag{12.4}$$

Note that the above expressions show that unless the rotation-translation coupling is strictly zero, it is not correct so simply invert the friction tensors to obtain the diffusion tensors – other authors have glossed over this fact (Carrasco and Garcia de la Torre 1999).

BEST computes diffusion tensors in the center of diffusion and the friction tensors in the center of resistance. Details have been presented (Aragon 2004). Furthermore, the more complex expressions for the computation of the intrinsic viscosity are available (Allison 1999; Hahn and Aragon 2006). In the paper by Hahn and Aragon, it is also shown that the center of viscosity is not equivalent to the center of diffusion and that a full matrix inversion is required to calculate the viscosity factor in the center of viscosity. These authors also found that the viscosity factor calculated at the body centroid is an excellent approximation to the true value for globular proteins. In centrosymmetric particles, all of these "centers" coincide.

12.2.2 Slip Boundary Conditions

In the case of slip boundary conditions, the normal component of the velocity of the fluid at the body surface is zero, but the tangential component is unconstrained. Thus, the fluid is said to "slip" past the body surface. This boundary condition has been typically used for small molecules diffusing in organic solvents and is not normally considered for macromolecular diffusion. We consider it here because in order to elucidate why the stick boundary condition is useful for macromolecules such as proteins, it will be convenient to consider the diffusion of the amino acid building blocks in water. In Sect. 12.3 this discussion will lead us to a reinterpretation and full understanding of the hydration parameter that all hydrodynamic modeling methods must use. Note that for two identical surfaces, the stick boundary condition causes greater amount of viscous energy dissipation (more drag) than the slip boundary condition. This effect can be easily observed in the exact computations for a sphere where D_T (stick)/D_T (slip) = 2/3 (Kim and Karilla 1991).

The integral equation for slip boundary conditions is more complex, requiring two integrals, the second of which also contains the unknown velocity of the fluid

at the body surface. It is given by (Kim and Karilla 1991; Odqvist 1930)

$$\begin{aligned}\frac{1}{2}\mathbf{u}(\mathbf{y}) &= \frac{1}{2}\mathbf{u}_0(\mathbf{y}) + \oiint \mathbf{T}(\mathbf{x},\mathbf{y}).\mathbf{f}(\mathbf{x})dS_x \\ &\quad -\frac{3}{4\pi}\oiint \frac{(\mathbf{x}-\mathbf{y})\mathbf{n}(\mathbf{x}).(\mathbf{x}-\mathbf{y})(\mathbf{x}-\mathbf{y}).\mathbf{v}(\mathbf{x})}{|\mathbf{x}-\mathbf{y}|^5}dS_x\end{aligned} \tag{12.5}$$

The normal unit vector to the surface at position $\mathbf{x}$ is denoted by $\mathbf{n}(\mathbf{x})$. The extra tensor that appears in this case is more singular than the Oseen tensor but causes no problems inside the integral. This equation can also be solved by discretization (Allison 1999). With slip boundary conditions, the tangential components of the surface stress $\mathbf{f}(\mathbf{x})$ are zero, and we have only N unknown normal components of $\mathbf{f}(\mathbf{x})$ for a surface divided into N triangles. Allison has shown (personal communication) that it is possible to eliminate the unknown velocity at the surface and obtain an equation for the normal components of the surface stress forces. In turn, these components suffice to compute the total force and torque on the body and thus the friction tensors. Using Eqs. (12.3) and (12.4), one can then compute the diffusion tensors as before. Allison's equation requires two matrix inversions to obtain the solution – the full derivation is omitted here – it is a clever modification of his previously published work (Allison 1999). The solution has been programmed in a Fortran program which enables computations with at most $N = 1000$ surface triangles. The regularization of the slip computations is a work in progress and we are limited to the treatment of small molecules at the present time. Nevertheless, the accuracy of this program has been demonstrated in several works (Allison 1999; Sturlaugson et al. 2010).

In the next section, we address the issue of the hydrodynamic hydration thickness, a parameter that is required for computed hydrodynamic transport properties to agree with experiment.

12.3 Hydrodynamic Hydration Reinterpreted

Hydrodynamics, the representation of a solvent as a continuum medium, is surprisingly effective in the description of the transport properties of large and small molecules, provided one uses an appropriate boundary condition at the surface of the solute molecule. For macromolecules such as proteins and nucleic acids dissolved in water, it is well known that the use of "stick" boundary conditions yields an excellent agreement with experimentally measured transport properties, as long as we assume that there is a thin hydration layer of about 1.1 Å thick around the macromolecule. In other words, the experimental diffusion coefficients are smaller than hydrodynamics predicted in the absence of "hydration." We describe the combination of stick boundary conditions and an empirical hydration parameter as a "hydrodynamic model." Such a hydrodynamic model is useful in the prediction of transport properties but we do not claim by its use that the water actually forms

a layer that moves with the protein as was believed by early workers (Kuntz and Kauzmann 1974; Squire and Himmel 1979). Yet the modern literature is still filled with claims that hydration water moves rigidly attached to the macromolecule. That naïve interpretation is simply not in agreement with the experimental fact that individual water molecules have a residence time at the surface of a protein in the 10 ps time scale, while rotational correlation times of proteins are in the 10 ns time scale and beyond. Magnetic relaxation dispersion (MRD) measurements of ^{1}H (Venu et al. 1997) and ^{17}O (Denisov and Halle 1996; Halle 1999) demonstrate that water molecules at a protein surface have mean residence times between 10 and 50 ps nearly independent of location on the protein surface. Molecular dynamics simulations come to the same conclusion (Makarov et al. 2000; Luise et al. 2000; Henchman and McCammon 2002). Thus, there must exist a dynamical effect at the protein surface that is mimicked by the presence of an immobile hydration layer.

A big step toward the correct interpretation was provided in a lucid paper (Halle and Davidovic 2003), hereafter denoted as HD. These authors noted that a plausible consequence of the perturbation of the solvent by a solute molecule is that the viscosity of the first solvation layer is different and larger from the bulk viscosity of the solvent. We shall see that an equivalent way of looking at this effect is to realize that there are extra sources of viscous energy dissipation at the protein surface layer. The Stokes creeping flow equations can be solved for rotation and translation of a sphere with such a thin layer of more viscous material around it with stick boundary conditions (Brilliantov and Krapivsky 1991). Let the bulk solvent viscosity be η_o, the viscosity of the thin layer be η_s, the sphere volume V_p, and the volume of the thin layer V_s. The volume of the thin layer can be well expressed by $V_s = A_p\ \lambda$, where A_p is the sphere area and λ the layer thickness. The results of the calculations can be expressed as the ratio of the diffusion coefficients with and without solvent perturbation and are given (without the approximations used by HD) by

$$D_R/D^o{}_R = 1-(1-\alpha)\ \ (1-<\eta_o/\eta_s>) \tag{12.6}$$

$$D_T/D^o{}_T = 1-(\lambda/\,(R+\lambda))\ \ \ (1-<\eta_o/\eta_s>) \tag{12.7}$$

for rotation (R) and translation (T), respectively, $\alpha = R^3/(R+\lambda)^3 = V_p/(V_p+V_s)$ $= 1/(1+\lambda\ r)$, and $r = A_p/V_p$. Note that these formulas have correct limits: if the layer thickness is zero, $\alpha = 1$, or if $b = 1$, the ratios are unity; if the layer viscosity is much larger than the bulk viscosity, then the last parenthesis is unity, giving a result with a geometrically larger size. In the above equations, I have inserted a spatial average of the viscosities in an anticipation of applying the sphere results to nonspherical solutes. For a water molecule, there is a direct relationship between the viscosity and the rotational correlation time $\tau = 1/6D_R \approx V\eta/kT$, where V is the water molecule volume. The relationship is missing a correct shape factor and a slip correction factor, but in the ratio $<\ \eta_o/\eta_s\ > = <\ \tau_o\,/\,\tau_s\ >$, such factors cancel out. Thus, as HD noted, the viscosity ratio can be related to a dynamical quantity that can be measured in a protein solution. HD further take into account

the distribution of relaxation times in a congested environment and obtain a simple relationship:

$$< \tau_o / \tau_s > = 2 \tau_o / < \tau_s > \tag{12.8}$$

Furthermore, HD argue that the shape effects are effectively the same for the unperturbed and the solvent perturbed case, so that the formulas (12.6) and (12.7) can be applied to globular proteins even though they are not exactly spherical. Now let's apply these relations with appropriate values for two cases that we will find useful to compare: lysozyme and glycine. Using the measured values of the parameters for these cases, we obtain the following ratios for the diffusion coefficients:

$$\text{Lysozyme} : V_p = 16 \text{ nm}^3, A_p = 64 \text{ nm}^2, \lambda = 0.2 \text{ nm}, < \tau_s >= 5.5 \tau_o$$
$$D_R/D^o{}_R = 0.72 \text{ and } D_T/D^o{}_T = 0.89$$

$$\text{Glycine} : V_p = 68.3 \text{ Å}^3, A_p = 89.7 \text{ Å}^2, \lambda = 2 \text{ Å}, < \tau_s >= 2.5 \tau_o$$
$$D_R/D^o{}_R = 0.86 \text{ and } D_T/D^o{}_T = 0.93$$

For both the protein and the amino acid constituent, the unperturbed diffusion coefficients are slowed down, and in the case of the proteins, the results agree well with experiment – the 30 % slowing in rotation is what is needed to match the measured values for lysozyme. HD and Aragon and Hahn have demonstrated that the result is accurate for proteins in general. For proteins, the 10 % decrease for translation also agrees with experiment. On the other hand, the results for glycine are in complete disagreement with experiment (note that the thin shell formulas make an insignificant error for a small molecule like glycine). For the moment, let's follow HD and compute the effective thickness that is required in order to mimic the dynamic solvent effect in a stick boundary condition calculation with a fixed solvent thickness δ. That is, we apply the standard hydrodynamic model by surrounding the protein with a layer of immobile water of thickness δ and computing the transport properties with stick boundary conditions. In this case, we will obtain a different expression for the ratios of diffusion coefficients with or without such hydration. Equating the relationship containing δ and that for Eqs. (12.6) and (12.7), we can solve for δ, in terms of the parameters of the dynamic perturbation model. The results for rotation and translation are

$$\delta_R \cong \frac{\lambda (1-b)\left(1-\frac{\lambda b}{R}\right)}{1+\lambda b/R} \tag{12.9}$$

$$\delta_T = \frac{\lambda (1-b)}{1+\lambda b/R} \tag{12.10}$$

In Eqs. (12.9) and (12.10) that I have derived with the aid of Mathematica, $b =< \tau_o/\tau_s >$. Equation (12.9) is an excellent approximation to the exact result and

Eq. (12.10) is exact. These expressions have two immediate consequences. First, the values of the thicknesses required for translation and rotation are predicted to differ, and second, the thicknesses depend on molecular weight (through the variable r) and temperature (through the variable b). If we use the approximate formulas quoted by HD that relate area and volume to protein molecular weight:

$$A_p = 7.43\ \mathrm{Mw}^{0.81}\mathrm{nm}^2,\ V_p = 1.02\ \mathrm{Mw}^{1.03}\mathrm{nm}^3 \tag{12.11}$$

and express $R = 3/\mathrm{r}$, the above formulas yield values of δ_R in the range of 1.18 Å for Mw = 300 kDa to 1.05 Å for Mw = 10 kDa, while for δ_T they yield 1.24 Å for Mw = 300 kDa to 1.18 Å for 10 kDa. Thus, the molecular weight dependence is only slight, and the value of the deltas for either case is almost the same and in remarkable agreement with the value of $\delta = 1.1$ Å found empirically in our work. Given all the approximations used above, the agreement can be taken as excellent.

Thus we arrive at the conclusion that the dynamical coupling of the protein with the solvent does indeed generate extra viscous energy dissipation which is manifest as increased viscosity in a thin layer around the protein. Before we return to the amino acid case, it is worth noting one other issue: the fact that this layer is predicted to be uniform over the entire protein surface. The key observation here is that (Harpaz et al. 1994) about 60 % of the protein surface is composed of atoms in hydrophobic residues, leaving only 40 % for potential preferential interaction sites. In addition, the MRD measurements of water residence times and the MD quoted previously show no significant variation over the entire protein surface.

Now we must discuss the relevance of the calculation of the transport properties of single components of a protein – the amino acids. In Table 12.1 we show the experimental values for the translational diffusion coefficient of three fairly rigid amino acids and the results of various hydrodynamic calculations. As input to the hydrodynamics, the zwitterionic amino acid structures were obtained with Spartan software (wavefunction.com) using Hartree-Fock with a 631 g* basis set. The triangulations were done with MSROLL using the united atom model, but hydrogens were not removed from the pdb files – the hydrogens are so small that this makes very little difference, given that the slip program has a typical 3 % error.

The immediately obvious result is that the stick boundary condition calculation fails in that the values are about 17 % lower than experiment, yet that calculation is the fastest possible result with stick boundary conditions because we have omitted

Table 12.1 Values of D_T for amino acids at 20 °C in water, 10^{-6} cm^2/s

Molecule	Stick unhydrated	Slip unhydrated	Slip 0.8 Å hydration	Experiment
Glycine	8.00	11.5	9.1	9.33[a]
Alanine	7.53	10.5	8.4	8.31[a],8.07[b]
Serine	7.31	10.2	8.2	8.17[a],7.75[b]

Stick unhydrated calculations done with BEST, slip calculations done with nutrn4 (Allison 1999)
[a]Ma et al. (2005)
[b]Germann et al. (2007)

all solvation. A full slip calculation with no hydration is too high, however. Thus we see that a slip boundary condition calculation requires a small layer of "solvation" in order to agree with experiment, as expected since water molecules do show slowed down rotational correlation times at the surface of amino acids (Halle 1999). For these cases we find that a value around 0.8 Å models the perturbation of the solvent adequately. The discrepancies with experiment are on the order of 3 %, which is the precision of the slip program and the experimental data. If we take the HD model at face value, we actually expect, as calculated previously, that the stick translational diffusion coefficient should be faster than experiment by about 7 %, yet we observe an opposite larger deviation. The fact that a slip hydrodynamic calculation better describes the diffusion of a small molecule is not a surprise – many previous workers have shown the appropriateness of such a change in boundary conditions when the solute is not much larger than the solvent (Bauer et al. 1974; Youngren and Acrivos 1975b). Thus we need to take this result seriously, for it is not an artifact of the continuum nature of hydrodynamics when applied to a smaller molecular scale.

Proteins, on the other hand, require a larger hydration layer on top of the slower stick boundary condition. Does a protein have an additional mechanism for viscous energy dissipation that a single amino acid does not have? In Fig. 12.1 we show the root mean square deviation of atoms in a protein as calculated by a molecular dynamics simulation on human serum albumin (1AO6.pdb). The MD simulation was carried out in explicit solvent after adding the missing residues to the crystal structure with Sali's Modeller program (Sali and Blundell 1993; Fiser et al. 2000) and preparing the molecule with the proper disulfide bonds with tleap in AMBER Tools 13 with the ff99SB force field of AMBER 12 (Case et al. 2012) using periodic boundary conditions in pmemd.cuda (Salomon-Ferrer et al. 2013) with a GTX 580 GPU. The simulation was carried out for 2 ns and data points were collected every 2 ps. The reference frame for the simulation was the first structure obtained after energy minimization and constrained heating steps. The figure, typical of any well-folded protein, shows us that the protein atoms on the average execute excursions of about 3 Å in position and that such excursions are already 2 Å by 50 ps, the characteristic residence time of water molecules near the surface. Thus, we see that the protein does have an additional mechanism for viscous energy dissipation that

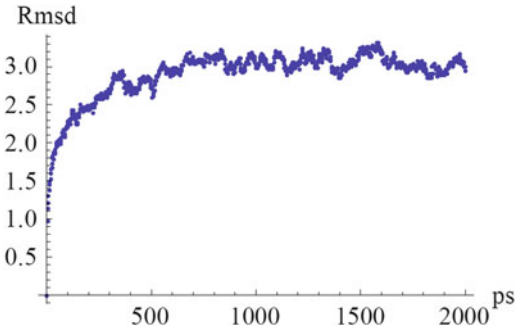

Fig. 12.1 The RMSD (average root mean square deviation in Å) of all atoms in human serum albumin (1AO6) from an arbitrary first frame. The diameter of a water molecule is 3 Å by comparison

is not present in the amino acids – the protein surface is dynamic! The protein is not rigid like our sample amino acids, and thus the protein atoms jostle the water molecules at the protein surface over the diameter of a water molecule. The entire first hydration layer on the protein is definitely disturbed, and this motion generates extra viscous energy dissipation. In other words, the reason we must use the slip boundary condition for a small molecule is that such tend to be nearly rigid and perturb the solvent little.

Our point of view can be clarified by considering the hypothetical case of a protein with no preferential interaction sites which was completely rigid. Then in that case, the interaction of water on its surface would be just the same as on a single rigid amino acid, and we would expect slip boundary conditions to be applicable for the hydrodynamics with a small solvation layer. The energy dissipation in that case would be determined by the geometric features of the protein surface and nothing else. The extent of the perturbation of the solvent would be somewhat larger than that of an amino acid due to more surface roughness. Note that the case of deeply buried water molecules causes no concern because such water molecules do not participate in viscous energy dissipation – only the free water molecules near the surface do. The real protein on the other hand definitely perturbs the water around it much more because of the dynamics of its surface atoms – it is not rigid. We have a layer of water in which extra energy dissipation occurs, thus the viscosity of that layer is larger, and as HD have shown, this slows down the diffusive motions of the macromolecule. Now there are two ways to materially make the calculations reflect this slowing down. One is to use *Slip* boundary conditions and a layer thickness of about 3 Å, considered as fixed hydration, or the alternative is to use *Stick* boundary conditions (which automatically increases the energy dissipation at the surface), and a much smaller thickness of fixed hydration, namely, 1.1 Å. Thus note that in this view, the use of stick boundary conditions and a fixed hydration layer is just a mimic of the effect of a layer in which additional viscous energy dissipation occurs at the protein surface due to its roughness and dynamics. As shown above, just considering how the rotation of water molecules is slowed down near the protein surface, one can calculate the 1.1 Å value that agrees with what BEST determined empirically.

This new view has several immediate consequences. First of all, it assigns the primary cause of the hydrodynamic hydration layer to protein surface atom motion, and thus predicts that the layer, to first order, should be uniform over the protein. The atoms of hydrophobic or hydrophilic residues move about the same. Any preferential interaction site is a perturbation on top of this picture. This perhaps explains why the uniform 1.1 Å parameter used in BEST works so well for monomeric proteins which tend to be very compact and well folded. On the other hand, it also predicts that multimeric proteins that have extra flexible loops or whose component chains can jiggle with respect to one another could need a higher value of the fixed hydration layer to account for a larger amount of solvent being perturbed due to this flexibility. The HD theory predicts that the hydration layer thickness should increase slightly with molecular weight and be temperature dependent. The extra dynamics in some multimeric proteins could add an additional factor. This can be tested with molecular dynamics simulations.

This new hydration interpretation also predicts something important for segmentally flexible proteins such as antibodies. If you have a protein composed of compact segments which move with respect to one another in time scales much longer than the residence time of water molecules on the surface of the protein, then the stick BC plus your standard 1.1 Å fixed layer will work just fine, provided you average the diffusion coefficients over an ensemble of shapes produced during an MD simulation. This was precisely demonstrated in our work with trastuzumab in 2010 where the agreement with experimental transport properties was excellent. This work is reviewed below. This new view also predicts that disordered proteins will require more hydration than the standard 1.1 Å with stick boundary conditions, due to the extra viscous energy dissipation provided by the flexible portions. Previous work (Rai et al. 2005) has also suggested a special role for the dynamics of flexible side chains in affecting the overall hydrodynamics of a protein, however, even though these authors were aware of the HD work, they did not quite make the connection with hydrodynamic boundary conditions that is highlighted here. In addition one can readily see that the amount of water that is involved in the thin 1.1 Å layer is not an accurate representation of the amount of water that is actually perturbed by the protein surface because the stick boundary condition has artificially imposed most of the extra energy dissipation. There is much more water than this layer indicates, and this helps to explain why "hydration water" measured in this way always comes out short (Aragon and Hahn 2006).

This new view also predicts that if you change the solvent, then you should be able to estimate the thickness of the layer by measuring the solvent rotational slowing at the macromolecule surface and that the layer thickness will depend principally on the solvent, and not the macromolecule (which contributes second-order effects). For solvents that are perturbed very little at the boundary with solute, little or no solvation will be needed in a hydrodynamic model and the appropriate boundary condition should be slip. Lastly, we can comment that hydrodynamics will be applicable as long as the solute size is larger than any free volume contained in the solvent, for otherwise, ballistic motion into such volumes can occur and the motion will be faster than predicted by hydrodynamics (Bauer et al. 1974; Sturlaugson et al. 2010).

To summarize: the introduction of a solute molecule into solvent perturbs the structure of the solvent at the solute boundary, thus increasing the solvent viscosity at the interface. The presence of the solute boundary is a wall that disrupts the solvent organization. If that wall has solvent size nooks and crannies, the solvent is perturbed a little more, and if the wall is not rigid, the largest amount of perturbation occurs. For amino acid-sized solutes, only the main smooth wall effect is present and the solvent perturbation is small, requiring the use of solvated slip boundary conditions. For macromolecules, the much larger perturbation is dominated by the solute surface dynamics and a convenient model is a solvated stick boundary condition.

12.4 Studies of Globular Proteins

We have previously reported on extensive calculations on proteins over a very broad range of molecular weight that show excellent agreement with experiment for the three basic transport properties using the same 1.1 Å hydration parameter.

This work has been previously reviewed (Aragon 2011) – here we mention only the salient points and update some of the work.

In the BE method, we need to define the "perturbed boundary" or "hydrated surface" of a protein, so an atomic resolution structure is a required input. In our previous work (Aragon and Hahn 2006; Hahn and Aragon 2006), where 49 proteins ranging from 9 to over 465 kDa where studied with BEST and stick boundary conditions, Connolly's program MSROLL (Connolly 1981, 1983, 1993) was used to roll a probe sphere of solvent size (1.5 Å) around the atomic arrangement defining the molecular surface, after all protein atoms have been "inflated" by 1.1 Å to account for the required hydrodynamic hydration. The atomic radii are only used to define the hydrodynamic surface to be triangulated. The fine triangulations produced by MSROLL are further processed by COALESCE (Aragon 2004), a program that can generate sub-triangulations, preserving the topological properties of the surface. A sample triangulation is shown in Fig. 12.2 (left) for ribonuclease. A sequence of such sub-triangulations with increasing numbers of triangles are analyzed by BEST to produce accurate transport properties via extrapolation to zero triangle size, as shown in Fig. 12.2 (right). The value of the hydration thickness was assigned by simply matching the measured translational diffusion coefficient of a set of four well-characterized small proteins (ribonuclease, myoglobin, lysozyme, and chymotrypsinogen) with the uniform increase in atomic size required for the computation to agree. Thereafter ALL proteins, large or small, were treated with the same value of the hydration parameter for all the transport properties.

The original work of Aragon and Hahn neglected to add missing residues in about 25 % of the proteins studied – the data presented in Table 12.2 for monomeric proteins has been corrected for such omission. It is clear that the agreement with

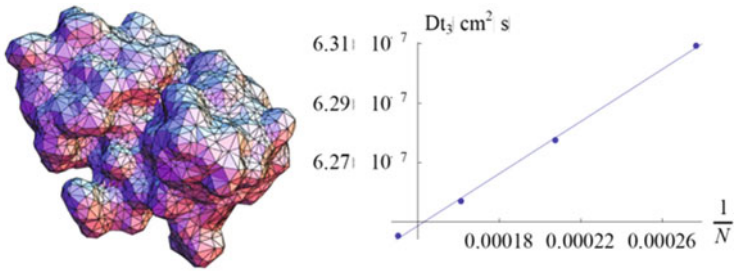

Fig. 12.2 *Left Panel*: Triangular tessellation of ribonuclease with 4952 triangles. *Right Panel*: The least squares fit line for the third eigenvalue of the translational diffusion tensor Dt extrapolation vs. 1/N of human serum albumin (1AO6)

Table 12.2 The intrinsic viscosity and translational diffusion coefficient of monomeric proteins

Protein	s^a	Mass (kDa)	$[\eta]$ (cm^3/g)			$D_t(10^{-7} cm^2/s)$		
			Calc	Exp.	Δ^b	Calc.	Exp.	Δ^b
Cytochrome C (1HRC)	1	12.4	3.07	2.74	13	11.63	11.1–12.1	0
Ribonuclease A (8RAT)	1	13.7	3.32	3.30,3.50	2.4	10.93	10.68	2.3
α-Lactalbumin (1A4V)	1	14.2	3.42	3.01, 3.4	6	10.74	10.57, 10.6	2
Lysozyme (1AKI)	1	14.3	3.14	2.66,3.0	11	11.08	10.6, 11.2	1.6
Myoglobin (1WLA)	1	17.2	3.15	3.25	3	10.10	10.4, 10.5	−3
Soyb.Tryp.Inhib. (1AVU)	1	20.1	3.18	2.8	14	9.88	9.8	1
β-Trypsin (1TPO)	1	23.3	2.99	3.1	4	9.58	9.3	3
Trypsinogen (1TGN)	1	24.0	3.00	2.96	1	9.49	9.68	−2
α-Chymotrypsin (4CHA)	1	25.2	3.25	3.00	8	9.11	9.33*	−3
Chymotrypsinog. A (2CGA)	1	25.7	3.20	2.5,3.13	4	9.16	9.23	−1
Carbonic anhyd. B (2CAB)	1	28.8	3.02	2.76,3.2, 3.7	−5	8.90	8.89	1
Zn-α2-Glycoprotein (1ZAG)	1	32.6	4.79	5.0	−4	7.30	7.96	−9
Pepsin (4PEP)	1	34.5	3.33	3.09,3.35	3	8.10	8.01, 8.71	−3
G-ADPActin (1J6Z)	1	43.0	3.92	3.7	6	7.43	7.15, 7.88	−1
Taka-amylase A (6TAA)	1	52.5	3.15	3.3	−3	7.22	7.37	−2
Human serum alb. (1AO6)	1	66.5	4.26	3.9, 4.2, 4.73	0	5.99	5.9, 6.1, 6.3	−2
Ovotransferrin (1OVT)	1	76.0	4.00	3.8	5	5.87	5.9	1
Lactotransferrin (1LFG)	1	77.1	4.00	4.0	0	5.85	5.6	4

[a]Number of subunits

[b]The percent difference between the calculated and experimental value determined from the average of the experimental values. References for experimental work are available in the original paper (Hahn and Aragon 2006)

experiment is excellent with the exception of 1ZAG whose *Dt* was recalculated from the reported sedimentation coefficient (Burgi and Schmid 1961). It is notable that the molecular weight calculated by these authors is high, possibly indicating the measured value of S is also high. It is also worth noting that the value of a more recent measurement of the sedimentation coefficient of ribonuclease (Moody et al. 2005) yields a value of *Dt* (with 8 % uncertainty) that conflicts with previous measurements quoted in Table 12.2, yielding a value 10 % higher. It is interesting that, as shown in Table 12.5, one cannot interpret this discrepancy as originating from a change of shape of ribonuclease upon going into solution because the molecular dynamics data agrees very well with the hydrodynamics of the crystal structure. The data of Moody et al. does show pH dependence, with data at lower pH tending to agree better with the hydrodynamics.

Table 12.3 The intrinsic viscosity and translational diffusion coefficient of multimeric proteins

Protein	s	Mass kDa	$[\eta]$ (cm^3/g) Calc.	Exp.	Δ^a	$Dt(10^{-7}$ $cm^2/s)$ Calc.	Exp.	Δ^a
Superoxide dismu. (2SOD)	2	32.5	3.57	3.3	9	8.10	8.27	−2
b-Lactoglobulin (1BEB)[b]	2	36.7	3.68	3.4–4.2	−3	7.72	7.3	6
a-Chymotrypsin (4CHA)	2	50.4	3.31	4.1,4.25	−21	7.16	7.1,7.4	−1
Concanavalin (1GKB)	2	51.4	3.60	4.1	−12	6.96	6.2	12
Triosephos. isom. (1YPI)	2	53.2	3.59	3.75	−4	6.80	6.76	6
Ricin (2AAI)	2	61.5	3.33	2.96	13	6.61	6.0	10
Oxyhemoglobin A (1HHO)	2	63.2	2.89	2.77	4	7.03	6.78	4
Alkaline phosphat. (1ALK)	2	94.6	3.09	3.4	−7	5.96	5.7	4
Citrate synthase (1CTS)	2	98.0	3.20	3.95	−20	5.82	5.8	0
Inorganic pyrophos. (1FAJ)	6	117.3	3.52	4.0	−12	5.33	5.7	−6
Aldolase (1ADO)	4	157.1	3.84	3.4,4.0,4.04	0	4.66	4.29–4.8	4
Catalase (4BLC)	4	235.7	3.01	3.9	−23	4.42	4.1	8
b-Galactosidase (1BGL)	4	465.8	3.84	3.78	2	3.26	3.13	4

s – number of subunits

[a]The percent difference between calculated and experimental values determined from the average of experimental values

[b]Heavy atoms only. References for experimental work are available in the original paper (Hahn and Aragon 2006)

The multimeric protein data of Aragon and Hahn is shown in Table 12.3. The few significant discrepancies with experiment for proteins found by these authors are worth mentioning in more detail. Whereas the computed transport properties of the 18 monomeric proteins treated as rigid objects generally agreed within experimental error (and the discrepancies were randomly distributed), there was a subset of 4 out of 13 multimeric proteins (α-chymotrypsin, citrate synthase, inorganic pyrophosphates, catalase) that showed large negative systematic deviations in the intrinsic viscosity exceeding –20 %. In addition, the translational diffusion data for the multimeric proteins shows mostly positive systematic deviations from experiment.

Note that the translational diffusion coefficient is a functional of shape divided by a characteristic length, the rotational diffusion tensor components are functionals of shape divided by a volume, but the intrinsic viscosity is exclusively a functional of shape and is thus the most sensitive of the measurements to changes in molecular shape. The results of our protein study indicated that for monomeric proteins, and most multimeric proteins, the crystal structure was a good representation of the average structure in solution. Given that there were only four very deviant cases out of 13 in the multimeric protein set, the most reasonable conclusion is that either the crystal structure and the average solution structure are significantly different for these proteins, or these proteins are significantly more flexible than others in the data set. The technique of molecular dynamics simulation in combination with hydrodynamic computations can be used to address these questions.

As mentioned previously, BEST is capable of computing transport properties to extremely high accuracy and statistical precision. For smooth surfaces, the accuracy is better than 0.02 %, while for amorphous molecular surfaces, the statistical precision is typically around 0.2 %. The ultimate limit in the precision is the accuracy of the atomic coordinates themselves. This limit is comparable also to the impossibility of defining the molecular surface to very high precision because doing so would require more than 20,000 triangles and that requires very large machine memories and much time for the computation. A practical limit for the values of transport coefficients, given these considerations, is about 1 % in translation and 2 % in rotation and intrinsic viscosity. These limits are still much better than most experimental uncertainties. The experimental data set could also be clearly improved. For example, the published *Dt* for Taka-amylase was not extrapolated to infinite dilution even though concentration data are presented in the paper. We have done the extrapolation and presented that improved value in Table 12.2. The 4CHA monomer was recently measured by analytical ultracentrifugation (Ghirlando 2011), and that greatly improved value is now presented in Table 12.2. There is a need for a carefully measured set of transport properties for proteins varying across the entire range of molecular weight – AUC would be an ideal technique to obtain accurate values of *Dt*.

12.5 Combination of Molecular Dynamics Simulation and Hydrodynamic Modeling

In the previous section, we described work in which proteins were assumed to be rigid objects with the crystal structure representing the average solution structure. This picture works very well for most proteins; however, we would like to know what effect the structural fluctuations present in solution have on the measured transport properties of globular proteins and also how to describe proteins that are flexible or have flexible subdomains. The technique of molecular dynamics (MD) simulation is well suited for this task. Modern-day parallel graphical processing units (GPUs) enable us to study even large-sized proteins with an explicit solvent simulation. MD work on the large multimeric proteins is ongoing in this laboratory to test the hypothesis that some have different structure in solution than in the crystal and also investigate their degree of flexibility.

12.5.1 Implicit Water MD of α-Chymotrypsin

One of the multimeric proteins that may have a significantly different structure in solution compared to the crystal is α-chymotrypsin. This protein has a dimer-monomer equilibrium that is pH dependent (Schwert and Kaufman 1951) and

was treated with AMBER's sander module (Version 9) at constant pH (Mongan et al. 2004) using an implicit solvent model. In an implicit solvent model, water is approximately represented by a continuum fluid with no viscosity, thus the dynamics occur much faster than in a real molecular system, allowing a short simulation to display significant changes. The protocol is similar to that of explicit water simulations described below. In addition, it is possible to choose a typical salt concentration for the system.

Constant pH implicit water simulations done at pH 7, where the protein exists as a monomer in solution, do indeed demonstrate that the initial crystal structure falls apart, and the two pieces separate in time (not shown). At pH 3, however, where the protein is a dimer in solution, the simulation keeps the protein together and deforms its shape, elongating somewhat as the simulation proceeds over 3 ns. The initial and a sample deformed shapes are shown in Fig. 12.3. The trajectory graphs for the translational diffusion coefficient and for the intrinsic viscosity are shown in Fig. 12.4. The graphs clearly show the deformation of the structure as the simulation proceeds as relaxation of the values occurs within the first 1–2 ns of trajectory. The transport properties computed as an average over the last 1 ns of simulation agree much better with experiment (Schwert and Kaufman 1951) than those of the crystal structure. The hydrodynamic analysis is shown in Table 12.4, where data

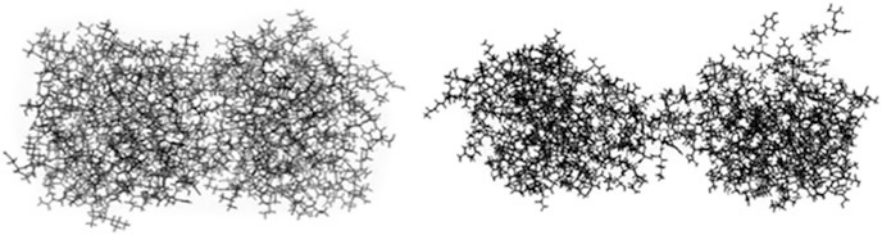

Fig. 12.3 α-chymotrypsin structures. *Left panel*: crystal structure (4cha.pdb). *Right panel*: AMBER 9 typical geometry after 1 ns molecular dynamics with implicit solvent at pH = 3.0 (Taken from Aragon 2011)

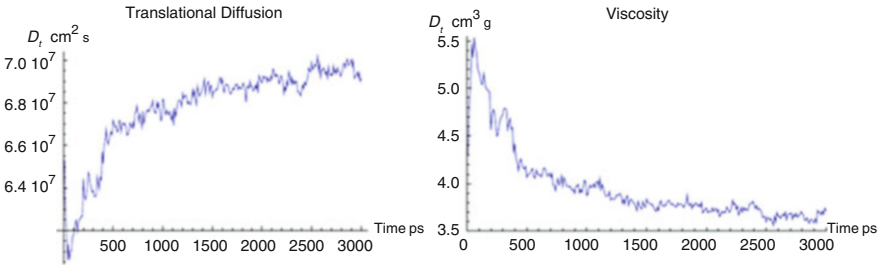

Fig. 12.4 The translational diffusion coefficient (*left panel*) and the intrinsic viscosity (*right panel*) of α-chymotrypsin (4CHA) from an MD trajectory with implicit water at pH 3.0. As the molecule shape deforms from the initial crystal structure, the transport properties evolve and settle down after 2.5 ns (Taken from Aragon 2011)

Table 12.4 The intrinsic viscosity and translational diffusion coefficient of α-chymotrypsin (4CHA) and β-lactoglobulin (1BEB) from implicit water MD

			$[\eta]$ (cm^3/g)			$Dt(10^{-7}$ $cm^2/s)$		
Geometry	n	Mass (kDa)	Calc.	Exp.	Δ	Calc.	Exp.	Δ
1beb.pdb	1	36.7	3.7	4.1[a]	−7.5	7.7	7.3[b]	5.5
Sander			**4.0**		−2.4	**7.5**		2.7
4cha.pdb	2	49.7	3.3	4.1[c]	−19	7.2	7.4[c]	−3
Sander			**3.7**		−10	**6.9**		−7

[a]McKenzie and Sawyer (1967)
[b]Ogston (1949)
[c]Schwert and Kaufman (1951)

for an additional monomeric protein, β-lactoglobulin, is shown as a control. Note that the D_t value of the α-chymotrypsin dimer was not corrected for concentration dependence and has a larger than normal uncertainty. The β-lactoglobulin MD results are only slightly improved from the crystal structure results, indicating that the force field is sufficiently accurate to model the system well. This is a result in the right direction but the implicit solvent model is a coarse representation of the aqueous medium.

What can we learn from a more realistic solvent model? Recently, the 4CHA simulations were repeated with explicit solvent MD (data not shown). To perform simulations without direct control of pH with explicit water solvent, the protein was titrated at pH 7 and 3 using the online pH – server module at the University of Virginia. Sufficient counterions were added to make the system neutral, but no extra ions were added to adjust toward an experimental ionic strength. The simulations were carried out to 20 ns with the protocols described below, but the results were not as expected. At pH 7, there was no indication that the protein dimer would separate into monomers. At pH 3, the prominent relaxation features in Fig. 12.4 were not seen – there doesn't appear to be a significant shape change during the simulation. AMBER 14 has just been released with new capabilities to carry out constant pH simulations with explicit water and this work will be repeated once more. On the other hand, the discrepancies could be due to greater than normal surface flexibility in this protein and further MD work should give us a clue.

12.5.2 Explicit Water MD of Small Proteins

Here we report on MD simulations of several small proteins, including some with flexible subdomains in order to validate the method for hydrodynamic computation. In our method, we generate a sequence of snapshots of the protein structure along a simulation trajectory or set of trajectories. Instead of trying to compute the transport properties directly from the trajectory (which requires very long trajectories), we simply compute the transport properties of each snapshot, taken as a rigid structure,

and then average over hundreds or thousands of snapshots, depending on how flexible the protein is. We call this the trajectory ensemble average method. We have used the AMBER (Versions 9,10,12) suite of programs (Perlman et al. 1995), and in particular the parallel program pmemd, to perform explicit water simulations with a TIP3P water model in an octahedral box with periodic boundary conditions. A typical simulation protocol consists of four steps: (1) energy minimization of the solvated system at constant volume and fixed protein coordinates to relax close contacts with solvent, (2) energy minimization of the entire system at constant volume with no restraints on the protein atoms, (3) 20 ps of MD simulation at constant volume with temperature increasing from 0 to 300 K with mild restraints on protein atoms, and (4) production run of MD simulation at constant pressure of 1 atm and temperature of 300 K with no restraints.

The first issue we must confront is the accuracy of the force fields that will yield the computed structures during the simulation. We have used three modern force fields that have been developed for accurate modeling of proteins: ff03, ff99SB, and more recently ff2012SB. These are compared in detail by Hornak et al. (2006) who show that ff03 performs slightly better for small systems such as ubiquitin, while ff99SB performs better for larger systems in the prediction of NMR order parameters which are sensitive to detailed local conformational structure. ff2012SB is a further improvement on ff99SB. In order to validate these force fields for whole molecule scale structure probed by hydrodynamics, we performed computations of small monomeric proteins whose crystal structure is a good predictor of solution structure and investigated whether this agreement is maintained during MD simulation. If the force field and simulation process are good, the agreement with experiment will be maintained.

Aragon and Hong have studied several small proteins with explicit water MD simulation (lysozyme, ribonuclease, bpti, human and mouse ubiquitin) using the AMBER pmemd parallel program with a protocol as described previously and an electrostatic cutoff that varied between 15 and 12 Å, depending on the size of the octahedral solvent box (Hong 2009). The solvent contained only as many ions to make the system neutral, but no added salt. The typical buffer used in experiments has a viscosity about 1 % higher than pure water and around 0.1 mM salt which serves to screen electrostatics. In addition, this work included a comparison with implicit water MD (not shown) on the same proteins and found a systematic discrepancy of about 15 % compared to explicit water simulations. The more salient points of the data obtained in this study will be reviewed here. Some of the transport properties of ribonuclease are shown in Fig. 12.5.

Note that, unlike the MD trajectory observed in Fig. 12.4 for α-chymotrypsin, the graph of the transport properties for ribonuclease along the trajectory does not show a relaxation at small times.

The graph fluctuates about the average from the initial points in the trajectory, indicating that the crystal structure is already close to the minimum energy in

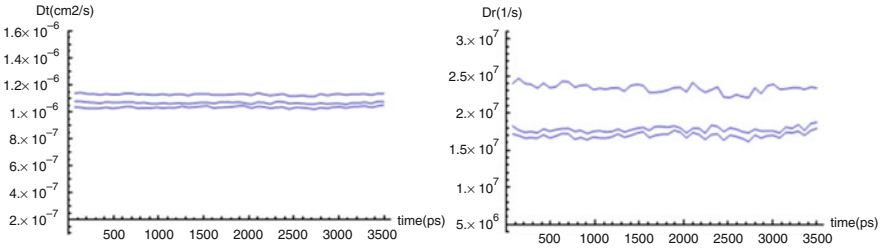

Fig. 12.5 *Left panel*: The translational diffusion tensor eigenvalues along the MD trajectory for ribonuclease (7RSA). Note the small difference between the eigenvalues, justifying the use of the average. *Right panel*: The rotational diffusion tensor eigenvalues along the MD trajectory. Note the symmetric top appearance of the eigenvalues. In both cases, the data shows only small thermal fluctuations characteristic of a globular protein

solution and the structure shows only thermal fluctuations, not a deformation. This result is typical of all the small proteins in this MD study. Average transport properties of lysozyme, ribonuclease, and human ubiquitin are shown in Table 12.5.

The first two molecules belong to the initial parametrization set for the determination of the hydration thickness of proteins from the translational diffusion coefficient, so the discrepancy between experiment and the crystal structure is much less than 1 %. It is noteworthy, however, that the MD simulation value for *Dt* also agrees to this level of precision, indicating that the ff03 force field is an excellent descriptor of the structure in solution. The agreement is less satisfactory for the intrinsic viscosity, but the experimental error in these determinations can vary between 5 and 10 %, making both the crystal structure values and the MD simulation values statistically equivalent.

The human ubiquitin molecule has a 6-residue end chain whose last 4 residues are quite flexible, compared to the fairly rigid structures of the other two proteins. However, despite this flexibility, the crystal structure is quite a good representative of the translational diffusion coefficient. In the crystal structure, the conformation of the chain sticks straight out of the molecule, while in the molecular dynamics structures, it is generally folded inward. The MD average intrinsic viscosity has a substantial difference with that from the crystal, but unfortunately we are not aware of an experimental measurement to make a fruitful comparison. This example shows that the translational diffusion coefficient is not very sensitive to small conformational changes in solution. The effects of shape can be offset by a change in size, leaving the value of *Dt* relatively unchanged. The intrinsic viscosity is sensitive only to shape and is a much better discriminator – the MD trajectory structures of ubiquitin show that only the last 4 residues, comprising about 5 % of the molecule, are actually flexible. In the case of ubiquitin, the table also shows that making the water model more realistic by using a four-point model yields insignificant change in the computed transport properties. Thus, we can conclude that a TIP3P water model yields an excellent descriptor of the conformations in solution even though

Table 12.5 Transport properties for lysozyme, ribonuclease, and ubiquitin

Protein	Data type	Intrinsic viscosity (cm^3/g)	Translational diffusion *Dt* (10^{-6} cm^2/s)	Rotational diffusion tensor Dr1 ($10^7/s$)	Dr2 ($10^7/s$)	Ave. Dr ($10^7/s$)
Lysozyme (6LYZ) 14.3 kDa	MD TIP3P	3.33 ± 0.01	1.09 ± 0.01	1.79 ± 0.01	2.52 ± 0.01	2.03 ± 0.01
	Crystal	3.21	1.10	1.82	2.57	2.07
	Exp.	298−3.00	1.11 ± 0.05	–	–	167 ± 0.08
			1.12 ± 0.02			2.0
			1.06 ± 0.01			
Ribonuclease (7RSA) 13.7 kDa	MD TIP3P	3.59 ± 0.01	1.08 ± 0.02	1.74 ± 0.1	2.34 ± 0.1	1.94 ± 0.1
	Crystal	3.39	1.10	1.83	2.50	2.05
	Exp.	3.30−3.50	1.068	–	–	2.01
Ubiquitin (1UBQ) 8002E6 kDa	MD TIP3P	3.54 ± 0.1	1.267 ± 0.003	2.75 ± 0.1	3.97 ± 0.1	3.16 ± 0.1
	MD TIP4P	3.57 ± 0.1	1.263 ± 0.002	2.73 ± 0.1	3.90 ± 0.1	3.16 ± 0.1
	Crystal	3.31	1.270	2.80	3.98	3.19
	Exp.		1.30 ± 0.01	3.17 ± 0.1	3.70 ± 0.1	3.34 ± 0.1

References to experimental work are available in Hong (2009)

the diffusion coefficient of water is more than twice the experimental value (Mark and Nilsson 2001). The timing of the dynamics is faster than in a real solution (allowing useful data to be obtained from shorter trajectories), but the range of structures thermally sampled is unaffected.

For the experimental rotational diffusion data for lysozyme in Table 12.5, at first glance it may seem that the two values imply a range of experimental error, but theoretically the value measured by fluorescence (Cross and Fleming 1986), which samples all the eigenvalues of the diffusion tensor, may be different from the depolarized dynamic light scattering value (Dubin et al. 1971). If the rotational diffusion tensor is diagonalized in the same principal axes system as the polarizability of lysozyme, then the birefringence value will not depend on the faster "axial" eigenvalue, called D_{r2} in Table 12.5. Aragon has also implemented a very accurate BE method (POL) for the solution of the electrostatic equations for the determination of classical polarizabilities (Aragon and Hahn 2007). Using the program POL, with the identical triangulation input file used for the hydrodynamics, it can be shown that both the polarizability and rotational diffusion tensor are diagonalized in essentially the same principal axes – despite its irregular shape, lysozyme is optically a symmetric top! Thus, the depolarized light scattering value should be compared to the average of the two smaller eigenvalues shown in Table 12.5 as D_{r1}. The MD value of $D_{r1} = 1.79\ 10^7\ s^{-1}$ is in good agreement with the light scattering experimental value of $1.67\ 10^7\ s^{-1}$ of Dubin et al. The fluorescence value samples all the eigenvalues because the transition moment is unlikely to be oriented along the principal axes of the rotational diffusion tensor. The fluorescence value $D_r = 2.0\ 10^7\ s^{-1}$ (Cross and Fleming 1986) compares very well with the average of the MD (2.03) or crystal structure (2.07) eigenvalues of D_r.

The MD simulations in explicit water appear to provide a very good description of the solution structure of small proteins as measured by hydrodynamic transport properties. Thus, in combination with the data from local structure provided by NMR order parameters, both the whole molecule scale structure and the local structure are well described by the ff03 force field. In the next section, we describe similar results for a large flexible protein.

12.5.3 Explicit Water MD Simulations of Trastuzumab

Brandt and coworkers have carried out explicit water MD simulations of a medium-sized flexible protein, trastuzumab, a monoclonal humanized IgG antibody produced by Genentech which is used in the treatment of breast cancer (Brandt et al. 2010). This study used the ff99SB force field of Simmerling and coworkers (Hornak et al. 2006) for its enhancement of the description of alpha helix secondary structure in proteins. The antibody is a larger flexible system (150 kDa) whose range of motion is very dependent on an accurate representation of the forces between atoms – the flexibility is due to a small hinge length of protein helix in the middle of the molecule. The simulation of trastuzumab required the construction of a

model from pieces that could be crystallized because flexibility has impeded the determination of the structure of the entire antibody by X-ray crystallography. The construction procedure relied on an approximate structure for the hinge postulated by Padlan (1994) and the in silico mutation of residues to make the model identical in atomic composition to trastuzumab. This initial construct was subject to energy minimization with the ff99 force field to eliminate construction artifacts, and subsequent 20 ns MD simulation with the TIP3P water model, using a protocol as described above for the small proteins. The final structure produced by that simulation was subsequently used in eight independent 40 ns (TIP3P, 300 K, 1 atm, 2 fs time step, SHAKE) simulations with ff99SB and Glycam04 force fields carried out in parallel in Genentech computer clusters. A snapshot of the trastuzumab structure from one of the independent simulations is shown in Fig. 12.6. The 0.34 μs piecewise trajectory was analyzed by computing the transport properties with the BEST suite, using a 1.1 Å uniform hydration model and compared to experiment. The transport properties were averaged over 3000 structures from the simulation, but separately for each subsimulation. The translational diffusion coefficient of trastuzumab was measured by dynamic laser light scattering and the intrinsic viscosity was measured by a rolling ball viscometer. Both measurements were carefully extrapolated as a function of concentration.

A summary of the results of this study are presented in Table 12.6. The values of the transport properties for each subsimulation are shown, along with the overall

Fig. 12.6 Ribbon structure of trastuzumab taken from one of the multiple MD trajectories (Aragon 2011)

Table 12.6 Summary of hydrodynamic analysis of trastuzumab MD simulation data, experimental hydrodynamic results, and literature values; 20 °C pure water

Trajectory	$Dt(10^{-7}$ cm^2/s)*	τ_r(ns)**	$[\eta]$ (cm^3/g)
Average[a]	4.08 (±0.07)	173 (±11)	6.24 (±0.3)
Experiment[b]	4.09 (±0.01)		6.37 (±0.2)
Literature[c]		168,180	6.20 (±0.5)

*For computational results: $Dt = \mathrm{Tr}(\mathbf{D}\mathrm{tt})/3$
**For computational results: $\tau_r = (6\mathrm{Dr})^{-1}$, where $\mathrm{Dr} = \mathrm{Tr}(\mathbf{D}\mathrm{rr})/3$
[a]For all MD data, values quoted are the average of eight trajectories and the standard deviation
[b]Uncertainties quoted are the standard error of extrapolations to $c = 0$
[c]See (Brandt 2010) for references to experimental values. Experimental τ_r values are for rabbit IgG and bovine IgG; intrinsic viscosity values are for human IgG1

average. It is immediately apparent that the experimental data and the simulation ensemble averages agree extremely well.

The MD simulation is able to determine the translational diffusion coefficient with a precision of 1.7 %, and it agrees with the experimental measurement to 0.25 %. The rotational correlation time was determined by MD to within 6.3 % and agreed with literature values for other IgG's to better than 5 %. Finally the intrinsic viscosity was determined to within 4.8 % and agreed with the measurement within 2 %, well within the measurement uncertainty of 3 %. The high precision of the experimental measurements and the high precision of the hydrodynamic computations are key components of the extremely good agreement observed in this study. The only other published MD study of a complete antibody in solution used much smaller length trajectories and did not make comparisons with experiment (Chennamsetty et al. 2009a, b). This study demonstrates that the force fields used generate an excellent representation of the solution structure of the antibody. The original paper (Brandt et al. 2010) contains a movie of the complete simulation trajectory in the published supplementary data, along with several figures showing the transport properties along the multiple MD trajectories.

12.6 Conclusions

The high precision implemented via the BE method in BEST has allowed us to generate a general model to numerically treat the transport properties of proteins with a single hydration parameter for all proteins regardless of size or flexibility. The hydration thickness of 1.1 Å is a model parameter that represents the increased viscosity of water around the protein when hydrodynamic stick boundary conditions are used. The dynamical origin of this parameter shows that the layer mimic should be uniform around the protein. The hydration model we have utilized allows for atomic size variation, unlike the approximate models of other authors (Garcia de la Torre et al. 2000b) who have proposed a single atomic equivalent radius (AER)

for all heavy atoms. A similar picture is obtained for nucleic acids as shown in a previous review (Aragon 2011), where it appears that DNA may have more hydration water in the grooves. Nevertheless, the recognition that macromolecular surface dynamics may be an important contributor to the increased viscous energy dissipation needs to be more thoroughly investigated.

Our studies of proteins led us to propose that some multimeric proteins have a conformational rearrangement upon going into solution from the crystal. Our preliminary work using MD simulation appears to bear this out, but the possibility of enhanced surface dynamics requiring a larger hydration parameter must still be considered. In order to validate that the structures generated by MD are actually representative of solution structure, we have performed simulations on a number of small proteins, rigid and flexible, and one medium-sized flexible protein. The good agreement we obtain with experiment demonstrates that we have validated both the force fields and the hydrodynamic hydration model for proteins. Our application with the precise hydrodynamics in BEST in combination with the trajectory ensemble average method yields very good agreement with experiment for both small and large proteins, flexible or not.

A large number of proteins have been studied by our group and others and there is broad agreement between experiment and computation, yet there remain several intriguing discrepancies. Some of these discrepancies may be due to older experimental data – it would be quite useful, using modern instrumentation such as AUC to produce a reference set of carefully measured transport properties in the near future.

Acknowledgments The author thanks David Hahn for performing implicit water MD for the α-chymotripsyn and β-lactoglobulin molecules. Financial support for some of the small protein and trastuzumab work was provided by Genentech. This work was funded in part by NIH grant GM52588 to S. Aragon and by the Center for Life Sciences at SFSU.

References

Allison SA (1999) Low Reynolds number transport properties of axisymmetric particles employing stick and slip boundary conditions. Macromolecules 32:5304–5312

Aragon SR (2004) A precise boundary element method for macromolecular transport properties. J Comput Chem 25:1191–1205

Aragon SR (2011) Recent advances in macromolecular hydrodynamic modeling. Methods 54:101–114

Aragon SR, Hahn DK (2006) Precise boundary element computation of protein transport properties: diffusion tensors, specific volume, and hydration. Biophys J 91:1591–1603

Aragon SR, Hahn DK (2007) Polarizability and Kerr constant of proteins by boundary element methods. Colloids Surf B Biointerfaces 56:19–25

Bauer DR, Brauman JI, Pecora R (1974) Molecular reorientation in liquids. Experimental test of hydrodynamic models. J Am Chem Soc 96:6840–6843

Bloomfield VA, Dalton WO, van Holde KE (1967) Frictional coefficients of multisubunit structures. I. Theory. Biopolymers 5:135–148; Ibid (1967) Frictional coefficients of multisubunit structures. II. Application to proteins and viruses. Biopolymers 5:149–159

Brandt JP (2010) Construction, molecular dynamics simulation, and hydrodynamic validation of an all-atom model of a monoclonal antibody. M.S. thesis, SFSU

Brandt JP, Patapoff TA, Aragon SR (2010) Construction, MD simulation, and hydrodynamic validation of an all-atom model of a monoclonal IgG antibody. Biophys J 99:905–913

Brenner H (1967) Coupling between the translational and rotational Brownian motions of rigid particles of arbitrary shape. II. General theory. J Colloid Interface Sci 23:407–436

Brilliantov NV, Krapivsky PL (1991) Stokes laws for ions in solutions with ion-induced inhomogeneity. J Phys Chem 95:6055–6057

Brookes E, Demeler B, Rosano C, Rocco M (2010) The implementation of SOMO (Solution MOdeller) in the UltraScan analytical ultracentrifugation data analysis suite: enhanced capabilities allow the reliable hydrodynamic modeling of virtually any kind of biomacromolecule. Eur Biophys J 39:423–435

Burgi W, Schmid K (1961) Preparation and properties of Zn-α2-glycoprotein of normal human plasma. J Biol Chem 236:1066–1074

Byron O (1997) Construction of hydrodynamic bead models from high- resolution X-ray crystallographic or nuclear magnetic resonance. Biophys J 72:408–415

Carrasco B, Garcia de la Torre J (1999) Hydrodynamic properties of rigid particles: comparison of different modeling and computational procedures. Biophys J 75:3044–3057

Case DA, Darden TA, Cheatham TE III, Simmerling CL, Wang J, Duke DE, Luo R, Walker RC, Zhang W, Merz KM, Roberts B, Hayik S, Roitberg A, Seabra G, Swails J, Goetz AW, Kolossváry I, Wong KF, Paesani F, Vanicek J, Wolf RM, Liu J, Wu X, Brozell SR, Steinbrecher T, Gohlke H, Cai Q, Ye X, Wang J, Hsieh MJ, Cui G, Roe DR, Mathews DH, Seetin MG, Salomon-Ferrer R, Sagui C, Babin V, Luchko T, Gusarov S, Kovalenko A, Kollman PA (2012) AMBER 12. University of California, San Francisco

Chennamsetty N, Helk B, Voynov V, Kayser V, Trout BL (2009a) Aggregation-prone motifs in human immunoglobulin G. J Mol Biol 391:404–413

Chennamsetty N, Voynov V, Helk B, Kayser V, Trout BL (2009b) Design of therapeutic proteins with enhanced stability. Proc Natl Acad Sci U S A 106:1937–11942

Connolly ML (1981) Molecular surface program. QCPE Bull 1:75–83

Connolly ML (1983) Analytical molecular surface calculation. J Appl Crystallogr 16:548–558

Connolly ML (1993) The molecular surface package. J Mol Graph 11:139–141

Cross AJ, Fleming GR (1986) Influence of inhibitor binding on the internal motions of lysozyme. Biophys J 50:507–512

Denisov VP, Halle B (1996) Protein hydration dynamics in aqueous solution. Faraday Discuss 103:227–244

Dubin SB, Clar NA, Benedek GB (1971) Measurement of the rotational diffusion coefficient of lysozyme by depolarized light scattering: configuration of lysozyme in solution. J Chem Phys 54:5158–5164

Durchschlag H, Zipper P (2003) Modeling the hydration of refinement and atomic models of proteins: prediction of structural and hydrodynamic parameters from X-ray diffraction and scattering data. Eur Biophys J 32:487–502

Fiser A, Do RK, Sali A (2000) Modeling of loops in protein structures. Protein Sci 9:1753–1773

Garcia de la Torre J, Bloomfield VA (1977a) Hydrodynamic properties of macromolecular complexes. I. Translation. Biopolymers 16:1747–1763

Garcia de la Torre J, Bloomfield VA (1977b) Hydrodynamic properties of macromolecular complexes. III. Bacterial viruses. Biopolymers 16:1779–1793

Garcia de la Torre J, Huertas ML, Carrasco B (2000a) Calculation of hydrodynamic properties of globular proteins from their atomic-level structure. Biophys J 78:719–730

Garcia de la Torre J, Huertas ML, Carrasco B (2000b) HYDRONMR: prediction of NMR relaxation of globular proteins from atomic-level structures and hydrodynamic calculations. J Magn Reson 147:138–146

Germann MW, Turner T, Allison SA (2007) Translational diffusion constants of the amino acids: measurement by NMR and their use in modeling the transport of peptides. J Phys Chem 111:1452–1455

Ghirlando R (2011) The analysis of macromolecular interactions by sedimentation equilibrium. Methods 54:145–156
Goldstein RF (1985) Macromolecular diffusion constants: a calculational strategy. J Chem Phys 83:2390–2397
Hahn DK, Aragon SR (2006) Intrinsic viscosity of proteins and platonic solids by boundary element methods. J Chem Theory Comput 2:1416–1428
Halle B (1999) Magnetic relaxation dispersion: principles and applications. In: Bellissent-Funel MC (ed) Hydration processes in biology. IOS, Amsterdam, pp 232–249
Halle B, Davidovic M (2003) Biomolecular hydration: from water dynamics to hydrodynamics. PNAS 100:12135–12140
Harpaz Y, Gerstein M, Chothia C (1994) Volume changes on protein folding. Structure 2:641–649
Henchman RH, McCammon JA (2002) Structural and dynamic properties of water around acetylcholinesterase. Protein Sci 11:2080–2090
Hong Q (2009) Molecular dynamics of small proteins in solution. MS. thesis, SFSU
Hornak V, Abel R, Okur A, Strockbine B, Roitberg A, Simmerling C (2006) Comparison of multiple Amber force fields and development of improved protein backbone parameters. Proteins 65:712–725
Hu CM, Zwanzig R (1974) Rotational friction coefficients for spheroids with the slipping boundary condition. J Chem Phys 60:4354–4357
Kang EH, Mansfield ML, Douglas JF (2004) Numerical path integration technique for the calculation of transport properties of proteins. Phys Rev E 69:031918-1–031918-10
Kim S, Karilla SJ (1991) Microhydrodynamics. Butterworth-Heinemann, New York
Kuntz ID Jr, Kauzmann W (1974) Hydration of proteins and polypeptides. Adv Protein Chem 28:239–345
Luise A, Falconi M, Desideri A (2000) Molecular dynamics simulation of solvated Azurin: correlation between surface solvent accessibility and water residence times. Proteins 39:56–57
Ma Y, Zhu C, Ma P, Yu KT (2005) Studies on the diffusion coefficients of amino acids in aqueous solutions. J Chem Eng Data 50:1192–1196
Makarov VA, Andres BK, Smith PE, Pettit BM (2000) Residence times of water molecules in the hydration sites of myoglobin. Biophys J 79:2966–2974
Mark P, Nilsson L (2001) Structure and dynamics of the TIP3P, SPC, and SPC/E water models at 298K. J Phys Chem A 105:9954–9960
McKenzie HA, Sawyer WH (1967) Effect of pH on β-lactoglobulin. Nature 214:1101–1104
Mongan J, Case DA, McCammon JA (2004) Constant pH molecular dynamics in generalized Born implicit solvent. J Comput Chem 25:2038–2048
Moody TP, Kingsbury JS, Durant JA, Wilson TJ, Chase SF, Laue TM (2005) Valence and anion binding of bovine ribonuclease A between pH 6 and 8. Anal Biochem 336:243–252
Odqvist FGK (1930) On the boundary value problems in hydrodynamics of viscous fluids. (German). Math Z 32:329–375
Ogston AG (1949) The Gouy diffusiometer: further calibration. Proc Roy Soc London 196:272–285
Oseen CW (1927) Hydrodynamik. Academiches Verlag, Leipzig
Padlan EA (1994) Anatomy of the antibody molecule. Mol Immunol 3:169–217
Perlman DA, Case DA, Caldwell JW, Ross WS, Cheathamm TE III, Debold FSD, Seibel G, Kollman GP (1995) AMBER, a package of computer programs for applying molecular mechanics, normal mode analysis, molecular dynamics and free energy calculations to simulate the structural and energetic properties of molecules. Comput Phys Commun 91:1–41
Rai N, Nollmann M, Spotorno B, Tassara G, Byron O, Rocco M (2005) SOMO (SOlutionMOdeler): differences between X-Ray and NMR-derived bead models suggest a role for side chain flexibility in protein hydrodynamics. Structure 13:723–734
Richards EG (1980) An introduction to physical properties of large molecules in solution. Cambridge University Press, London

Rotne J, Prager S (1969) Variational treatment of hydrodynamic interaction in polymers. J Chem Phys 50:4831–4837

Sali A, Blundell TL (1993) Comparative protein modelling by satisfaction of spatial restraints. J Mol Biol 234:779–815

Salomon-Ferrer R, Goetz AW, Poole D, Grand S, Walker RC (2013) Routine microsecond molecular dynamics simulations with AMBER – Part II: particle Mesh Ewald. J Chem Theory Comput 9:3878–3888

Schuck P (2000) Size-distribution analysis of macromolecules by sedimentation velocity ultracentrifugation and lamm equation modeling. Biophys J 78:1606–1619

Schwert GW, Kaufman S (1951) The molecular size and shape of the pancreatic proteases. III. α-Chymotrypsin. J Biol Chem 190:807–816

Spotorno B, Piccinini L, Tassara G, Ruggiero C, Nardino M, Molina F, Rocco M (1997) BEAMS (BEAds Modelling System): a set of computer programs for the generation, the visualization and the computation of hydrodynamic and conformational properties of bead models of proteins. Eur Biophys J 24:373–384

Squire PG, Himmel ME (1979) Hydrodynamics and protein hydration. Arch Biochem Biophys 196:165–177

Sturlaugson AL, Fruchey KS, Lynch SR, Aragon SR, Fayer MD (2010) Orientational and translational dynamics of polyether/water solutions. J Phys Chem 111:5350–5358

Teller DC, Swanson E, de Haen C (1979) The translational friction coefficients of proteins. Methods Enzymol 61:103–124

Venable RM, Pastor RW (1988) Frictional models for stochastic simulations of proteins. Biopolymers 27:1001–1014

Venu K, Denisov VP, Halle B (1997) Water ^{1}H magnetic relaxation dispersion in protein solutions. A quantitative assessment of internal hydration, proton exchange, and cross-relaxation. J Am Chem Soc 119:3122–3134

Wegener WA (1986) On an exact starting expression for macromolecular hydrodynamic models. Biopolymers 25:627–637

Youngren GK, Acrivos A (1975a) Stokes flow past a particle of arbitrary shape: a numerical method of solution. J Fluid Mech 69:377–402

Youngren GK, Acrivos A (1975b) Rotational friction coefficients for ellipsoids and chemical molecules with the slip boundary condition. J Chem Phys 63:3846–3848